Interaction sizes of the even neodymium isotopes from elastic α scattering*

S. L. Tabor,† B. A. Watson,‡ and S. S. Hanna
Department of Physics, Stanford University, Stanford, California 94305
(Received 20 January 1976)

Differential cross sections for α particles elastically scattered from ^{142,144,146,148,150}Nd have been measured at six angles over the energy region 11–19 MeV. The cross sections were analyzed using the optical model, the incoming-wave boundary condition model, and the coupled-channels model. The radius at which the real nuclear potential is 2% of the Coulomb potential was found to be effectively independent of the ambiguities in the optical potential. In the coupled-channels analysis, the radius at which the spherically averaged real nuclear potential is 2% of the spherically averaged Coulomb potential is almost identical, for a given nucleus, to the corresponding quantity determined using the spherical optical model. The absolute increase in the "2% radius" over the neodymium isotopes is about 2 times larger than the increase in the charge distribution as observed in muonic-atom and electron-scattering studies.

[NUCLEAR REACTIONS ^{142,144,146,148,150}Nd(α, α); E = 11–19 MeV; measured $\sigma(E, \theta)$. Deduced nuclear interaction size. Enriched targets.]

I. INTRODUCTION

The possibility of measuring properties of the nuclear matter distribution from elastic alpha particle scattering has attracted a number of workers. Jackson and Morgan,[1] who examined the optical model ambiguities for alpha scattering, concluded that the mean square radius of the interaction potential is ambiguously determined and that the potentials which fit the data equally well are equal at the strong absorption radius. Several microscopic calculations have been made relating matter densities to optical model potentials.[2] Batty and Friedman[3] have applied the microscopic model to elastic scattering of alpha particles from the lead isotopes in order to relate nuclear matter distributions to the Coulomb barrier radii measured by Goldring et al.[4] Eisen[5] has combined a microscopic and phenomenological analysis of ^{16}O scattering on the isotopes of calcium to extract nuclear matter differences.

A detailed analysis of the onset of strong interaction effects in the elastic scattering cross section yields information on the tail of the nuclear matter distribution. Size measures obtained in this way will be called "interaction sizes". This technique has previously been employed to measure relative interaction sizes of the isotopes of lead,[4] calcium[6] and tin.[7] The relative sizes of the isotopes of a given element can be measured with greater precision and fewer uncertainties in interpretation than can their absolute sizes.

The object of the present investigation is to determine the differences in nuclear interaction sizes among the even isotopes of neodymium through analysis of elastic α scattering in the region of the Coulomb barrier. Also, the Nd isotopes provide an opportunity to study the role of deformation in the determination of nuclear sizes, since the deformation ranges from $\beta = 0.104$ for ^{142}Nd to $\beta = 0.279$ for ^{150}Nd.[8] In addition, since ^{142}Nd has a closed neutron shell, the effect on the interaction size of adding neutrons to an empty shell can be investigated.

Since a spherical optical model analysis was used in previous size studies of this type, we apply the optical model to the results of the present experiment. We then analyze the elastic data using the coupled-channels model to represent properly the deformed nuclear potential. The parameters of the deformed potential determined from the coupled-channels calculation can then be compared to those determined from the spherical optical model. The comparison provides some insight into the usefulness and limitations of the simpler spherical optical model for the description of elastic scattering from deformed targets.

Finally, the results can be compared with with the charge distribution sizes of the same Nd isotopes obtained from electron scattering studies[9] and from measurements of x ray line shifts from muonic atoms.[10]

II. EXPERIMENTAL TECHNIQUE

The elastic alpha scattering cross sections were measured simultaneously at laboratory angles of $\pm 30°$, $-70°$, $\pm 90°$, $+120°$, $+140°$ and $+165°$ as a function of incident energy in the range 11 to 19 MeV. The alpha energy was varied in 0.5 MeV steps in a sequence with undisturbed scattering geometry and a single target. The process was repeated for each isotope.

With typical beam currents of 100 to 200 nA of α^{++} particles, the live times of data accumulation were 98% or greater. Signals from the eight silicon surface barrier detectors were mixed into two analogue-to-digital converters (ADC's) in groups of four. Counting rates in the two ADC's were balanced so that their live times were very similar. The spectra were routed into appropriate sections of an on-line PDP-7 computer memory with a program which allowed on-line spectrum integration. Overall α resolution was typically 75 keV.

For each energy of observation, the number of scattered particles detected at each angle was divided by the average number detected in the 30° counters. Within the uncertainties of the unnormalized data, the 30° scattering below 19 MeV was found to be Rutherford. Furthermore, optical-model calculations indicate that the cross section at 30° should be Rutherford to within 0.5% over the energy range of interest. Thus, each normalized yield is essentially proportional to the ratio of actual cross section to what it would be in the absence of nuclear forces. The constants of proportionality were determined at the lowest beam energies where the cross sections could be ascribed to Rutherford scattering.

Use of the 30° scattering normalization eliminated uncertainties arising from beam integration, target thickness and target nonuniformity. Statistical accuracy was maintained at 1% or better. The major source of error was due to small shifts in the position of the alpha beam on the target when the beam energy was changed. These shifts affect the scattering angles of the detectors and are "amplified" by the strong angle dependence of the Rutherford cross section at forward angles. The use of two 3 mm diam collimators separated by 1.1 m in the beam line in front of the scattering chamber considerably reduced the beam shifts. The counters at ± 30° and ± 90° served to monitor and provide corrections for these shifts.

Isotopically enriched targets of ^{142}Nd, ^{144}Nd, ^{146}Nd, ^{148}Nd and ^{150}Nd were prepared by evaporating 100 to 150 μg/cm^2 (40 μg/cm^2 for ^{150}Nd) of NdF_3 onto a backing of approximately 100 μg/cm^2 of aluminum. The NdF_3 was formed by successive addition of HCl and HF to Nd_2O_3, the chemical form in which enriched isotopes of Nd were supplied by Oak Ridge National Laboratory. Attempts to use a carbon backing were unsuccessful.

III. RESULTS

Complete resolution of the elastic neodymium peak from other peaks in the spectrum was necessary to obtain the required accuracy of the measurements. Inelastic groups were well separated from the elastic peak except for the first 2^+ state at 132 keV in ^{150}Nd. The use of a thinner target improved the energy resolution to an acceptable level for this isotope. The contamination (a few per-

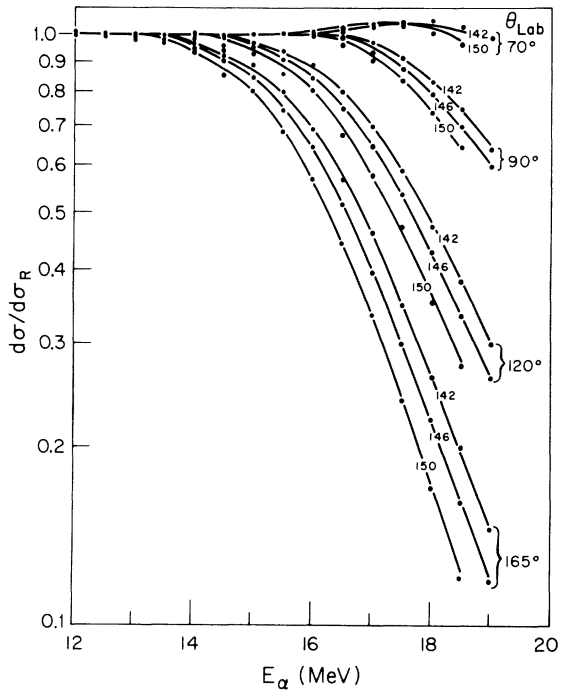

FIG. 1. Elastic alpha scattering cross sections relative to charge scattering cross sections as a function of laboratory energy. Target mass numbers are indicated on the optical model fits which are shown as solid lines.

cent) from isotopes of Nd other than the selected one in the target was not a significant source of error because of the small change of cross section among the isotopes. All other elements in the target were light and scattering from them was kinematically resolved at all angles from that from Nd.

Examples of the measured cross section ratios are shown in Fig. 1. Results for 140° and for ^{144}Nd and ^{148}Nd are suppressed for clarity. This graph shows that departure from charge scattering is a smooth function of energy and that the effect of increasing the neutron number of the target is largely a displacement along the abscissa. Spacing between isotopes is substantially greater than the fluctuations in the measured cross sections.

It was shown in Ref. 7 that the deviation from Rutherford scattering on the tin isotopes is approximately a function of the classical distance of closest approach. The cross section ratios for α scattering on ^{144}Nd are graphed as a function of the distance of closest approach in a pure Coulomb field (r_{min}) in Fig. 2. It can be seen that very little dependence on the scattering angle remains in the case of Nd as well. Thus it appears that the characterization of the elastic scattering cross section by r_{min} may be a general feature of elastic scattering just above the Coulomb barrier.

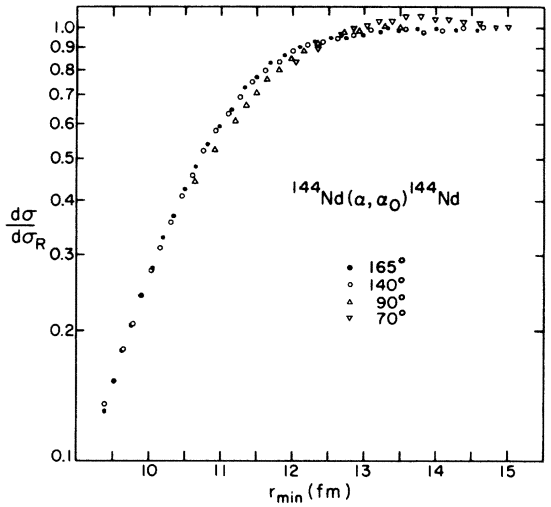

FIG. 2. Elastic alpha scattering cross sections relative to charge scattering cross sections for ^{144}Nd as a function of classical distance of closest appraoch in a pure Coulomb field.

IV. OPTICAL MODEL AND INCOMING-WAVE BOUNDARY ANALYSIS

For purposes of comparison we have analyzed the data using the spherical optical model (OM). Since the analysis procedure has been described,[7] only a brief outline will be presented here. The same spherical Woods-Saxon shape has been used for both the real and imaginary nuclear potentials and the strength of the imaginary potential was fixed at 10 MeV. For a fixed value of the real potential strength V_0, the Woods-Saxon radius and diffuseness parameters R and a were varied separately for each isotope to yield the best agreement between calculated and measured cross sections. Since the experimental accuracy was limited by factors other than statisics, χ^2 was calculated by assigning a 1% uncertainty in the data and by normalizing to the number of degrees of freedom.

The results of the OM analysis are presented in Table I. Potential depths of 50 and 100 MeV give approximately equally good fits, as does 150 MeV for the one case tried. A potential strength of 200 MeV gives noticeably poorer fits in most cases. This ambiguity in V_0 extending from below 50 MeV to about 150 MeV demonstrates that the experiment is not sensitive to the potential in the nuclear interior. Some typical fits can be seen in Fig. 1. The smooth lines in this figure are the results of the OM calculations using the parameters in Table I for V_0 = 100 MeV.

The OM fits are quite insensitive to simultaneous changes in R and a of opposite sign. To illustrate this point, Fig. 3 shows a locus of constant χ^2 plotted in the parameter space of relative R and a. Since χ^2 changes most slowly along the major axis of the ellipse of Fig. 3, the size parameter which is constant along

TABLE I. Parameters for the optical model and incoming-wave boundary condition (IWB) model which yield the best agreement with the measured elastic cross sections.

Nd isotope	R_0 (fm)	a (fm)	V_0[a] (MeV)	χ^2	r_R (fm)	R_{cf} (fm)
142	7.905	0.5620	50	0.85	10.110	10.737
144	8.000	0.5630	50	1.09	10.221	10.843
146	7.950	0.5814	50	0.38	10.225	10.888
148	8.005	0.5840	50	0.78	10.296	10.960
150	7.957	0.6160	50	1.87	10.345	11.081
142	7.625	0.5430	100	0.82	10.168	10.740
144	7.730	0.5420	100	1.28	10.282	10.844
146	7.670	0.5590	100	0.35	10.285	10.884
148	7.725	0.5620	100	0.89	10.359	10.960
150	7.670	0.5910	100	1.92	10.416	11.078
144	7.585	0.5310	150	1.08	10.318	10.852
142	7.290	0.5340	200	1.49	10.176	10.723
144	7.490	0.5230	200	1.74	10.345	10.859
146	7.297	0.5556	200	1.29	10.290	10.877
148	7.312	0.5644	200	2.31	10.350	10.952
142		0.5160	IWB	0.74	10.225	10.727
144		0.5190	IWB	1.03	10.330	10.833
146		0.5340	IWB	0.66	10.345	10.878
148		0.5380	IWB	1.26	10.415	10.953
150		0.5670	IWB	2.53	10.475	11.071

[a] W_0 = 10 MeV for the optical model fits.

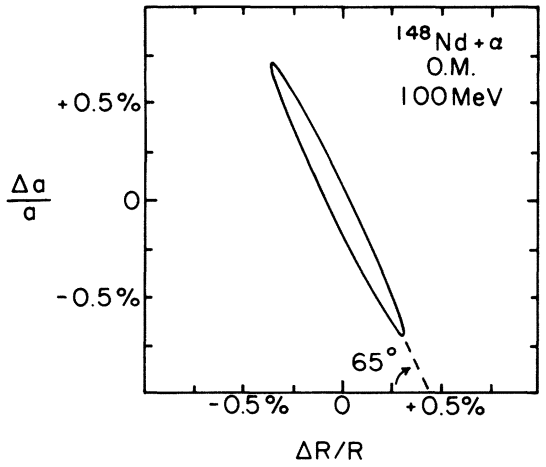

FIG. 3. A contour of constant χ^2 as a function of the parameters R and a varied for the fit to data of alpha scattering from ^{148}Nd for an optical model potential depth of 100 MeV.

this line is the one best determined by the fit.

One parameter which is rather well determined[4,6,7] by elastic scattering near the Coulomb barrier is the "Rutherford radius" r_R. This is the radius at which the total real potential (Coulomb plus nuclear) achieves its maximum. Rutherford radii for the Nd isotopes are listed in Table I and displayed in Fig. 4. It is evident from this graph that the change in r_R as a function of mass number A is similar for the two choices of V_0. However, the absolute values of r_R do depend slightly on V_0. The line of constant r_R in the parameter space of R and a lies at an angle of 75° to the R axis and is not quite parallel to the major axis of Fig. 3.

It was shown in Ref. 7 that the radius R_{cf} at which the real nuclear potential is 2% of the strength of the Coulomb potential is optimally determined. The values of these "2% radii" are included in Table I. They are essentially independent of V_0. In addition, the line of constant R_{cf} lies at an angle of 67° to the R axis of Fig. 3 and is almost parallel to the major axis of the χ^2 ellipse. It is this minimal dependence on both the R vs. a and the V_0 ambiguities of the fit which indicates that R_{cf} is the optimally determined parameter in this experiment. We will return to the discussion of this size measure in Sec. VI.

The accuracy to which the parameters are determined in this model was estimated by separately fitting two sets of data recorded several months apart on each of two isotopes (144 and 148). The error limit for each parameter was defined by

$$\delta P = \mathrm{Max}(\Delta P_{144}/\sqrt{2}, \Delta P_{148}/\sqrt{2})$$

where ΔP_A is the difference between the two parameters P which best fit the two sets of data measured on the neodymium isotope of mass A. For a fixed value of V_0 these error estimates are

$$\delta R = 0.064 \text{ fm}, \quad \delta r_R = 0.025 \text{ fm},$$

$$\delta a = 0.011 \text{ fm}, \quad \delta R_{cf} = 0.009 \text{ fm}.$$

Error bars reflecting these values are shown in Figs. 4 and 5. They are reasonable estimates for the relative accuracy among the isotopes. However, the error bars in Fig. 4 do not include the effect of the ambiguity in V_0 and errors in the absolute sizes are difficult to assess.

The incoming-wave boundary condition (IWB) model of Eisen and Vager[11] was used for comparison with the OM. The IWB model includes the effect of strong absorption directly in its formulation by assuming that, interior to a certain radius, the projectile wave function has only incoming components. This permits[7] the use of a purely real spherical nuclear potential with only two free parameters. The results of the IWB analysis are listed in Table I with the notation "IWB" in the V_0 column. It is evident from the values of χ^2 that this model describes the elastic scattering as well as the OM does.

The Rutherford radii, which are used as an input parameter in the IWB model, are displayed in Fig. 4. The curve of r_R as determined by the IWB model is parallel to that of r_R determined by the OM for a

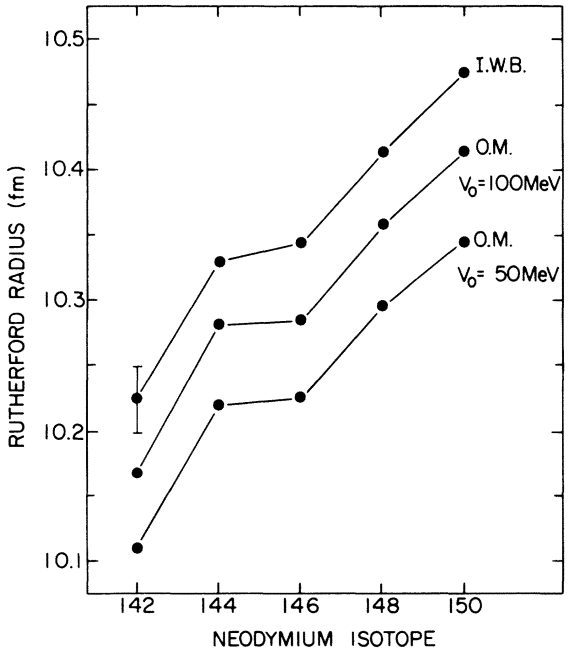

FIG. 4. Rutherford radius as a function of mass number in the neodymium isotopes. Lines are drawn connecting points calculated from the parameters which best fit the data for the optical model (OM) with the indicated well depths and for the incoming wave boundary condition model (IWB).

constant value of V_0. This fact provides a justification for our use of fixed values of V_0 in the OM analysis. The 2% radii R_{cf} can also be calculated from the IWB potentials and are included in Table I.

V. COUPLED CHANNELS ANALYSIS

Elastic scattering from deformed nuclei is better treated by the use of a deformed interaction potential with the resultant coupling of inelastic scattering to the elastic one. In this analysis we have used the coupled channels (CC) code Jupitor[12] of Tamura with the following nuclear and Coulomb potentials:

$$V_N(r,\theta,\phi) = \frac{-(V_0 + iW_0)}{1 + \exp\{[r-R(\theta,\phi)]/a\}} \quad (1)$$

and

$$V_C(r,\theta,\phi) = ZZ'e^2 \int \frac{\rho(r',\theta',\phi')}{|\vec{r} - \vec{r}'|} d\vec{r}' \quad (2)$$

with

$$R(\theta,\phi) = NR_0[1 + \beta Y_{20}(\theta,\phi)] \quad (3)$$

and

$$N = \left[1 + \frac{3}{4\pi}\beta^2 + \frac{1}{7\pi}\sqrt{\frac{5}{16\pi}}\beta^3\right]^{-1/3} . \quad (4)$$

The charge distribution $\rho(r,\theta,\phi)$ is taken to be constant within the volume defined by $R(\theta,\phi)$ and zero outside. The factor N is introduced to make the volume enclosed by the surfaces of constant V_N independent of the nuclear deformation β. The other symbols have their usual meanings.

For simplicity we have considered only the dominant inelastic process, scattering to the lowest $J^\pi = 2^+$ state. The calculation includes the effects of Coulomb excitation to the 2^+ channel as well as the channel coupling introduced by the deformed nuclear potential.

The values of the deformation parameter β deduced[8] from Coulomb excitation measurements of the $B(E2,0^+\rightarrow 2^+)$ transition strengths were used. Although our experiment was not optimized for measuring inelastic cross sections, the predictions of the coupled channels code, using these values of β and the Woods-Saxon parameters which best fit the elastic cross sections, are in good agreement with the available inelastic data from the present experiment.

In the coupled channels analysis V_0 and W_0 have been fixed at 100 and 10 MeV, respectively. The justification for using a constant value of V_0 for the OM was pointed out in the preceding section. The parameters R_0 and a were varied separately for each isotope to achieve the best agreement between measured and calculated cross sections. The results of this analysis are presented in Table II. Good fits were obtained for all of the isotopes except ^{150}Nd, which produced a significantly larger χ^2.

It is difficult to compare the CC and OM parameters meaningfully because the former represent a deformed potential while the latter are derived from a spherically symmetric potential. Because the experiment is sensitive to the fringe of the nuclear potential, it is more instructive to compare the OM surface parameters r_R and R_{cf} with similar parameters derived from the CC nuclear potential averaged over the sphere. That is, we define

$$\bar{V}_N(r) = \frac{1}{4\pi}\int V_N(r,\theta,\phi)d\Omega \quad (5)$$

and

$$\bar{V}_C(r) = \frac{1}{4\pi}\int V_C(r,\theta,\phi)d\Omega \quad (6)$$

where $V_N(r,\theta,\phi)$ and $V_C(r,\theta,\phi)$ are given in Eqs. (1)-(4) above. The two surface size parameters can then be calculated from these spherically averaged potentials:

$$\frac{d}{dr}\{\bar{V}_C(r) + \mathrm{Re}[\bar{V}_N(r)]\}\Big|_{r=r_R} = 0 \quad (7)$$

and

$$\mathrm{Re}[\bar{V}_N(R_{cf})] = -0.02\bar{V}_C(R_{cf}) . \quad (8)$$

The expansions of V_N and V_C in powers of β which were used in the present analysis are

TABLE II. Parameters for the coupled-channels model which yield the best agreement with the measured elastic sections with V_0 = 100 MeV and W_0 = 10 MeV.

Nd isotope	R_0 (fm)	a (fm)	β[a]	χ^2	r_R (fm)	R_{cf} (fm)
142	7.546	0.5432	0.104	1.09	10.170	10.744
144	7.556	0.5550	0.111	1.08	10.239	10.834
146	7.441	0.5685	0.161	1.31	10.244	10.873
148	7.376	0.5790	0.197	1.45	10.282	10.934
150	7.004	0.6400	0.279	6.96	10.234	11.039

[a]Reference 8.

$$V_N(r,\theta,\phi) = \frac{1}{\sqrt{4\pi}} f^0(r) + f^1(r)\beta \sum_\mu \mathscr{D}^1_{\mu 0} Y_{1\mu}(\theta,\phi) \tag{9}$$

with

$$f^\lambda(r) = -4\pi \int_0^1 \frac{V_0 + iW_0}{1 + \exp\{[r - R_0(1+\beta Y_{20}(\theta'))]/a\}} Y_{\lambda 0}(\theta')\, d(\cos\theta') \tag{10}$$

and

$$V_C(r,\theta,\phi) = \frac{ZZ'e^2}{r} + \frac{3ZZ'e^2}{5} \frac{R_0^2}{r^3} \beta \sum_\mu \mathscr{D}^2_{\mu 0} Y_{2\mu}(\theta,\phi) \tag{11}$$

outside the charge distribution.

The calculation of Eqs. (5) and (6) with (9) - (11) is straightforward. The first terms of Eqs. (9) and (11) are independent of (θ,ϕ) and survive unchanged in the integration. Because of the orthogonality of the spherical harmonic functions, the second terms of Eqs. (9) and (11) vanish when averaged over the sphere. Hence,

$$\overline{V}_N(r) = -\int_0^1 \frac{V_0 + iW_0}{1 + \exp\{[r - R_0(1+\beta Y_{20}(\theta'))]/a\}} d(\cos\theta') \tag{12}$$

and

$$\overline{V}_C(r) = \frac{ZZ'e^2}{r} \tag{13}$$

outside the charge distribution. To determine r_R and R_{cf} from the Woods-Saxon parameters we have solved Eqs. (7) and (8) numerically using Eqs. (12) and (13). For each value of r, Eq. (12) was integrated numerically.

The resulting size parameters are included in Table II. As a function of A, the Rutherford radii r_R determined from the spherically "averaged" CC analysis are similar to but somewhat more constant than those determined from the OM, while the 2% radii R_{cf} determined in the two analyses are almost identical. The similarity of its values in the OM and the averaged CC model gives further proof that R_{cf} is the size parameter that is best determined in this experiment.

VI. CONCLUSIONS

In summary, it is apparent from Fig. 1 that significant differences in elastic α scattering from the Nd isotopes have been observed. For a given isotope, the departure of the elastic cross section from the Rutherford value is approximately a function only of the distance of closest approach, as shown in Fig. 2. Although ambiguities exist among the parameters determined by the three analyses - OM, IWB, averaged CC - the radius R_{cf} at which the real nuclear potential is 2% of the Coulomb potential is almost independent of these ambiguities.

Because it is optimally determined in this experiment, we confine the following discussion to the interaction parameter R_{cf}. The most important observation concerning R_{cf} is that, in addition to being almost independent of the ambiguities of each model, it is also almost independent of which model is used. The agreement between values of R_{cf} in the

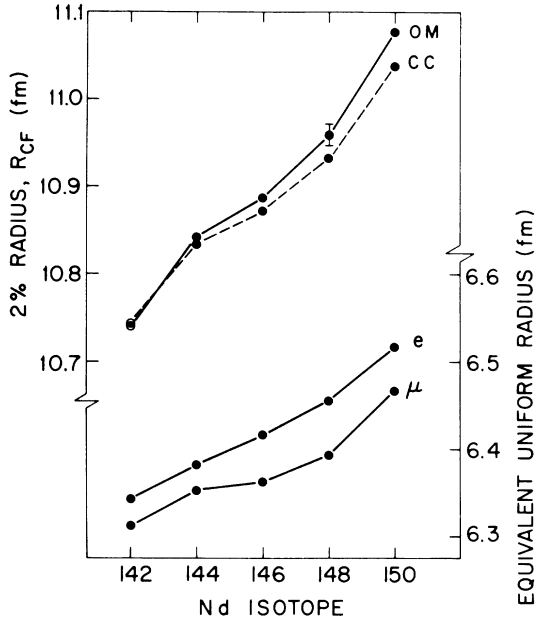

FIG. 5. Size measurements of the neodymium isotopes determined by elastic scattering of electrons and α particles and from line shifts in x rays from muonic atoms. The charge sizes are equivalent uniform radii. Those determined by electron scattering (Ref. 9) are labeled by "e" and those determined from muonic atoms (Ref. 10) are labled by "μ". The values of R_{cf} determined in the present work from the optical model and coupled channels analysis are labeled by "OM" and "CC", respectively. The validity of comparing charge and potential sizes is discussed in the text.

spherical model and the averaged deformed model was not entirely expected. It apparently indicates that, under the conditions of the present experiment, the scattering cross section from a spherical potential is almost identical to that from a deformed one which has the same average over the sphere.

The usefulness of R_{cf} as a nuclear size measure deserves some comment since radial moments, such as $\langle r^2 \rangle$, are more commonly used. Unlike electron and nucleon scattering, the scattering of heavier ions near the Coulomb barrier is not sensitive to the more interior regions of the nuclear potential which determine the mean square radius. In this experiment we have measured essentially the distance at which the nuclear force begins to modify the Coulomb scattering. From this perspective, a size measure such as R_{cf} which depends on the relative magnitude of the two potentials at the fringe of the nuclear potential appears reasonable. The best fraction (2% in this case) probably depends on the extent of the region above the Coulomb barrier over which the elastic cross sections are measured.

A direct comparison of the results of the present work with previous measurements of the mean square radius of the Nd charge distributions is difficult because R_{cf} is directly related to the interaction potential and only indirectly to the matter distribution. Changes in the size of the nuclear matter distribution will certainly affect the extent of the potential field, but detailed knowledge of the distribution would be needed to establish the exact relationship. However, a visual comparison of the values of R_{cf} with those of the charge sizes is informative.

The values of R_{cf} determined from the optical model and from the averaged coupled channels model are shown in Fig. 5. The sizes of the charge distributions determined from electron scattering[9] and from muonic atom x rays[10] are included in this figure. The charge sizes shown are the radii of uniform distributions which have the same mean square radii as those determined in the experiments. One can conclude that the fringe of the nuclear potential increases in size more rapidly (on an absolute basis) than does the equivalent uniform charge radius. As noted above, knowledge of the shapes of the distributions would be needed to establish whether this implies that the size of the nuclear matter distribution increases more rapidly than does the charge distribution. On the other hand, any description of the matter distributions of the Nd isotopes must produce agreement with the results of this experiment as to the extent of the nuclear potentials. It is interesting to note that the increase in R_{cf} when two neutrons are added to the closed neutron shell in ^{142}Nd is not much larger than when they are added to the partially filled shells in the other Nd isotopes.

The authors are pleased to acknowledge the continuing interest in these experiments of G. Goldring and informative discussions with him and Y. Eisen.

---

*Supported in part by the National Science Foundation.

†Present address: Physics Division, Argonne National Laboratory, Argonne, Illinois 60439.

‡Present address: Lockheed Palo Alto Research Laboratory, Palo Alto, California 94304.

[1] D. F. Jackson and C. G. Morgan, Phys. Rev. 175, 1402 (1968).

[2] D. F. Jackson and V. K. Kembhavi, Phys. Rev. 178, 1626 (1969); A. Budzanowski, A. Dudek, K. Grotowski, and A. Strzalkowski, Phys. Lett. 32B, 431 (1970); A. M. Bernstein and W. A. Seidler, Phys. Lett. 34B, 569 (1971); P. Mailandt, J. S. Lilley, and G. W. Greenlees, Phys. Rev. Lett. 28, 1075 (1972).

[3] C. J. Batty and E. Friedman, Phys. Lett. 34B, 7 (1971).

[4] G. Goldring, M. Samuel, B. A. Watson, M. C. Bertin, and S. L. Tabor, Phys. Lett. 23B, 465 (1970).

[5] Y. Eisen, Phys. Lett. 37B, 33 (1971).

[6] M. C. Bertin, S. L. Tabor, B. A. Watson, Y. Eisen, and G. Goldring, Nucl. Phys. A167, 216 (1971).

[7] S. L. Tabor, B. A. Watson, and S. S. Hanna, Phys. Rev. C11, 198 (1975). In this paper the measured size parameter was referred to as the matter radius. However, since it is only one of several possible measures of the matter distribution, we have adopted the term interaction size in the present paper.

[8] P. L. Stelson and L. Grodzins, Nucl. Data A1, 21 (1965).

[9] J. H. Heisenberg, J. S. McCarthy, I. Sick, and M. R. Yearian, Nucl. Phys. A164, 340 (1971).

[10] E. R. Macagno, S. Bernow, S. C. Cheng, S. Devons, I. Duerdoth, D. Hitlin, J. W. Kast, W. Y. Lee, J. Rainwater, C. S. Wu, and R. C. Barrett, Phys. Rev. C1, 1202 (1970).

[11] Y. Eisen and Z. Vager, Nucl. Phys. A187, 219 (1972).

[12] T. Tamura, Rev. Mod. Phys. 37, 679 (1965).